厚生労働科学研究費補助金

感覚器障害研究事業

蝸牛内の外有毛細胞に発現するタンパク質モータPrestinの活性部位の探求に関する研究：Prestin改変による感音難聴とその治療戦略

平成17年度　総括研究報告書

主任研究者　　和田　仁

平成18（2006）年　4月

目次

厚生労働科学研究費補助金（感覚器障害研究事業）

総括研究報告書

蝸牛内の外有毛細胞に発現するタンパク質モータPrestinの活性部位の探求に関する研究：Prestin改変による感音難聴とその治療戦略

主任研究者　和田　仁　東北大学　教授

研究要旨

我々の聴覚の鋭敏さは，蝸牛内コルチ器に存在する外有毛細胞（Outer Hair Cell: OHC）の伸縮運動により実現されていると考えられている．また，その伸縮運動の源は，細胞側壁に存在するタンパク質モータ Prestin の変形であると推察されている．現在，内耳疾患の治癒率が低い最大の原因は，内耳増幅機構，すなわち，OHC の伸縮メカニズムが不明なためである．従って，OHC の伸縮運動の源である Prestin の機能を明らかにし，OHC の駆動メカニズムに関する重要な知見が得られれば，OHC 機能不全由来の内耳疾患の原因解明及びその遺伝子治療などにつながると考えている．

本研究は遺伝子工学的手法を用いて，Prestin の機能発現に重要な役割を果たしている部位の同定を目指す．昨年度までに Prestin の機能に重要であることを明らかにした，N 末端細胞内領域，STAS（Sulphate Transporters and Antisigmafactor Antagonists）ドメイン及び GTSRH 配列への変異導入による Prestin が受ける糖修飾の変化を，脱糖鎖酵素処理により調べた．また，Prestin 特有のアミノ酸である 122 番目のメチオニン（M）をイソロイシン（I），192 番目のシステイン（C）をアラニン（A），225 番目のメチオニン（M）をグルタミン（Q），415 番目のシステイン（C）をアラニン（A），428 番目のスレオニン（T）をロイシン（L）にそれぞれ変異させ，その陰イオン輸送機能をパッチクランプ法により評価した．

分担研究者氏名・所属機関名及び所属機関における職名

小林俊光・東北大学・教授

熊谷 泉 ・東北大学・教授

池田勝久・順天堂大学・教授

津本浩平・東京大学・助教授

A. 研究の背景と目的

図 1 にヒトの耳の模式図を示す．空気の疎密波である音は，外耳道を通り，鼓膜を振動させる．この振動はツチ骨，キヌタ骨，アブミ骨よりなる耳小骨連鎖を経て，内耳蝸牛に伝えられる．蝸牛内はリンパ液で満たされており，アブミ骨より伝えられた振動は，リンパ液の圧力変動へと変換される．

蝸牛内をらせん状に走る基底板の上にはコルチ器という器官が存在する（図 2）．上述のリンパ液の圧力変動により，コルチ器は上下に振動する．コルチ器には，内有毛細胞（IHC）と，外有毛細胞(OHC)と呼ばれる 2 種類の感覚有毛細

胞が存在し，コルチ器の振動により，有毛細胞上端に存在する聴毛が屈曲する．IHC では聴毛の屈曲に伴って，そこに存在するイオンチャンネルが開き，陽イオンが流入する．これにより細胞内電位が上昇し，聴神経を発火させる．この信号が脳へと伝達されることで，我々は音を認識する．もう一つの感覚有毛細胞である OHC ではコルチ器の振動に伴い，IHC と同様に細胞内電位が変化する．この電位変化を感知し OHC は自らの細胞長を変化させる．この細胞長変化はコルチ器の振動を増幅する．この増幅機構により我々は鋭敏な聴覚を得ている．

OHC は図 3 のように円筒形をしており，その半径は 4−5 μm, 長さは 20−90 μm である．OHC の側壁は細胞膜，細胞骨格，subsurface cisternae の三層からなる．細胞膜にはタンパク質モータが密に存在し，このモータが細胞内外の電位差に応じてその立体構造を変化させ，上述の細胞長変化を実現していると考えられている．2000 年に Zheng らによってこのタンパク質モータの遺伝子が同定され, Prestin と命名された. さらに, Liberman らは，聴性脳幹反応の閾値が Prestin ノックアウトマウスでは，野生型のマウスに比べて上昇することを示した．これは Prestin が，聴覚の鋭敏性に重要な役割を果たしていることを示している．また，2003 年に遺伝性難聴を引き起こすヒト Prestin 遺伝子の変異が報告された. 分子的観点から見ると, Prestin はその遺伝子配列から分子量が約 82 kDa, 744 残基の膜貫通型タンパク質であり，陰イオン輸送体（SLC26A）のスーパーファミリーのメンバーであると考えられている(図 4).

我々の聴覚において，OHC による蝸牛増幅機構は重要な役割を果たしている．しかし，この OHC は一度消失すると再生しない．また，老人性難聴は OHC の機能低下およびその一部の脱落によると考えられている．現在，内耳疾患の治癒率が低い最大の原因は，内耳増幅機構，すなわち, OHC の伸縮メカニズムが不明なためである．従って，聴覚にとって重要な役割を果たしている OHC の伸縮運動の源を担っている，タンパク質モータ Prestin の機能を明らかにし，OHC の駆動メカニズムを解明することは内耳疾患の原因解明及びその治療にとって重要な意味を持つ．本研究では遺伝子工学的手法を用いて, Prestin の機能発現に重要な役割を果たしている部位の同定を目指す.

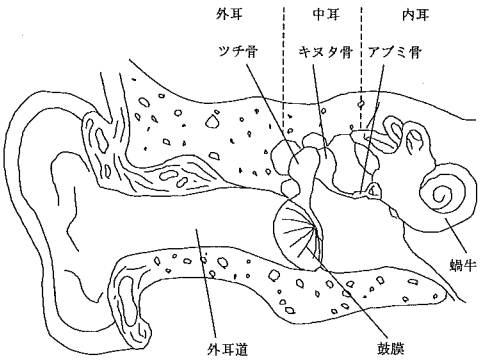

図 1. ヒトの耳の模式図.

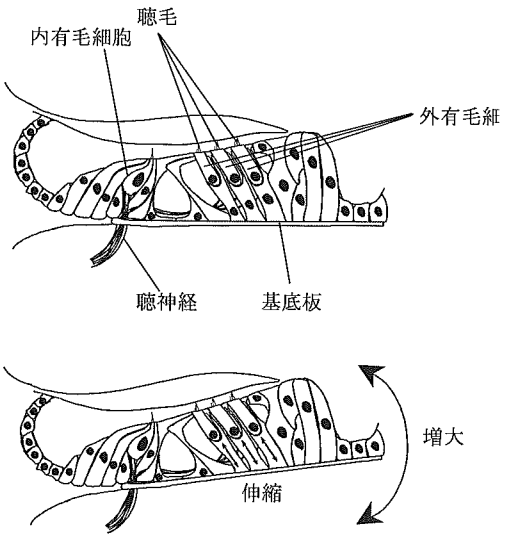

図 2. コルチ器と外有毛細胞によるその振動増幅．外有毛細胞の伸縮運動によりコルチ器の振動は増幅される.

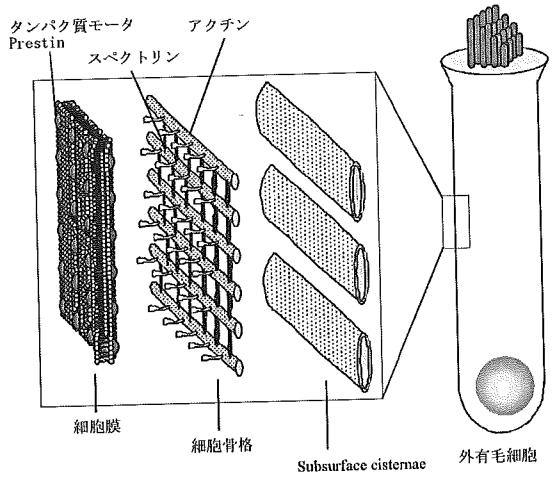

図 3. 外有毛細胞の模式図. 外有毛細胞の側壁は 3 層からなり，一番外側の細胞膜にタンパク質モータ Prestin が存在する.

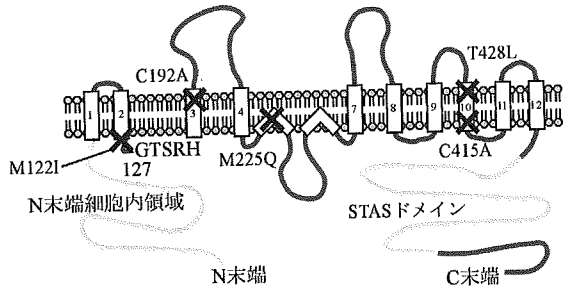

図 4. タンパク質モータ Prestin の 2 次構造予測図.

B. 研究方法

B. 1. GTSRH への変異と糖修飾の関係

B. 1. 1. 哺乳類細胞への遺伝子導入

昨年度までに，Prestin の機能発現に重要な部位であることが示された N 末端細胞内領域，STAS ドメイン及びグリシン（G），スレオニン（T），セリン（S），アルギニン（R），ヒスチジン（H）からなる GTSRH 配列の変異が，Prestin が受ける糖修飾に及ぼす影響を脱糖鎖処理により調べた．実験には HEK293 細胞を用いた．細胞は 10%ウシ胎児血清，100 U penicililin/ml，100 μg streptmycin/ml を加えた RPMI-1640 培養液を用いて培養した．N 末端細胞内領域欠損 Prestin，STAS ドメイン欠損 Prestin, G127A, T128A, S129A, R130A, H131A 及び S129T の遺伝子はそれぞれ LipofectAMIN2000（Invetrogene）を用いて，HEK293 細胞に導入した．本研究で用いた，発現ベクターpIRES-hrGFP-1a（図 5）には Green fluorescent protein (GFP)の遺伝子が挿入されており，遺伝子導入の有無は GFP の緑色蛍光を蛍光顕微鏡で観察することで確認できる.

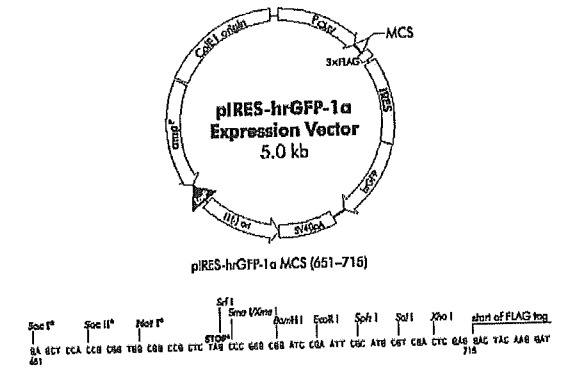

図 5. 哺乳類発現ベクターpIRES- hrGFP-1a.

B. 1. 2. 脱糖鎖処理

脱糖鎖酵素として，Endo H 及び PNGase を用いた．Endo H は小胞体で付加される高マンノース型糖鎖のみを，PNGase は高マンノース型及び，ゴルジ体で付加されるすべての複合型糖鎖を消化する．GFP の発光により Prestin の発現を確認した HEK293 細胞を Endo H または PNGase により処理し，以降の実験に用いた.

B. 1. 3. Western blotting

脱糖鎖処理した HEK293 細胞を用い SDS-PAGE 及び Western blotting を行った．細胞を溶解し，10%ポリアクリルアミドゲル電気泳動で，分子量ごとに分離し，タンパク質をニトロセルロース膜に転写した．抗 FLAG 抗体及び HRP 標識抗マウス IgG 二次抗体を用いて

Prestinを標識し，化学発光により検出した．

B. 2. Prestinに特有なアミノ酸の機能解明

B. 2. 1. Prestinに特有なアミノ酸への変異導入

OHC の伸縮運動を引き起こす電位依存性の構造変化は Prestin 特有である．そのため，Prestin が属する SLC26A ファミリーの他のタンパク質と比較し，Prestin のみに存在するアミノ酸がその特性に重要な役割を果たしている可能性が高い．本研究では，SLC26A ファミリーに属するタンパク質の全アミノ酸配列を比較し，Prestin 特有のアミノ酸である，122 番目のメチオニン（M），192 番目のシステイン（C），225 番目のメチオニン（M），415 番目のシステイン（C），428 番目のスレオニン（T）に注目した．これらのアミノ酸の役割を調べるために，M122 をイソロイシン（I），C192 をアラニン(A)，M225 をグルタミン(Q)，C415 をアラニン（A），T428 をロイシン（L）へとそれぞれ変異させた．

変異遺伝子作製には Overlap extension PCR 法を用いた．野生型 Prestin 遺伝子を鋳型とし，上流側領域と下流側領域を変異させたいアミノ酸をコードするコドン付近で 30bp ほど重複するように増幅させた．この際，プライマーにより，対象のコドンを変異させた(表 1, 5′ end forward, M122I reverse 及び M122I forward, 3′ end reverse 等)．こうして得られた 1 次 PCR 産物を混合し，2 次 PCR を行うことで，重複部位で 2 種類の PCR 産物は接合し，増幅する．PCR 産物および哺乳類発現ベクター pIRES-hrGFP-1a（図 5）を，制限酵素 *Bam*HI と *Eco*RI により消化後，この 2 つを T4 DNA ligase を用いて結合させた．反応後のプラスミドベクターを，大腸菌 JM109 株を用いてクローニング，増幅し，精製した．構築した発現ベクターの挿入部分の塩基配列を，DNA シーケンサーABI PRISM 310（Applied Biosystems）を用いて確認した．

（倫理面への配慮）

本研究には組換え DNA 実験が含まれる．組換え DNA 実験に関しては「遺伝子組換え生物等の使用等の規制による生物の多様性の確保に関する法律」に基づき，学内委員会にて組換え DNA 実験計画書の承認を得た上で安全性に最大限の配慮をし，実験を行った．

B. 2. 2. パッチクランプ法による機能評価

HEK293 細胞に発現した Prestin の活性を評価するため，パッチクランプ法により，電位依存性膜容量を計測した．Prestin が存在する細胞では，膜容量がベル型と呼ばれる電位依存性の非線形性を示すことが知られており，計測によってベル型の非線形膜容量が計測されるか否か，及び計測されたベル型の形で Prestin の活性を評価できる．

計測には Axopatch 200B パッチクランプ用アンプ（Axon Instruments）を使用し，pCLAMP 8.0 ソフトウェアの membrane test モードを利用して，膜電位を-140 mV から+70 mV まで変化させた時の膜容量を計測した．電極はボロシリケイト管より作製した，アクセス抵抗が 2-4 MΩのもの用いた．ピペット内溶液の組成は 140 mM CsCl, 2 mM $MgCl_2$, 10 mM EGTA, 10 mM HEPES, pH 7.2 である．また，細胞外溶液は 120 mM NaCl, 20 mM TEA-Cl, 2 mM $CoCl_2$, 2 mM $MgCl_2$, 10 mM HEPES, 5 mM glucose, pH 7.2 のものを用いた．

遺伝子導入から 24-48 時間後に蛍光顕微鏡 TE300（NIKON）を用いて，GFP の蛍光が観

表 1. 変異体作製に用いたプライマーの配列

Name	Sequence
3′ end reverse	5′ GGAATTCTTATGCCTCGGGTGTGGTGG 3′
5′ end forward	5′ CGGGATCCATGGATCATGCCGAAGAAAAATG 3′
M122I forward	5′ CCTGTTATCATATACTGTTTCTTTGGGACC 3′
M122I reverse	5′ GGTCCCAAAGAAACAGTATATGATAACAGG 3′
C192A forward	5′ GAATCATTCAGTTTGCCCTAGGTGTGTGC 3′
C192A reverse	5′ GCACACACCTAGGGCAAACTGAATGATTC 3′
M225Q forward	5′ CACGTCTTCACATCCCAGTTGAAATACCTG 3′
M225Q reverse	5′ CAGGTATTTCAACTGGGATGTGAAGACGTG 3′
C415A forward	5′ CACAGCTCGCAGGTGCCTTGGCCTCGCTG 3′
C415A reverse	5′ CAGCGAGGCCAAGGCACCTGCGAGCTGTG 3′
T428L forward	5′ GGTCATTTTAGCCCCTGGATTCCTCTTTG 3′
T428L reverse	5′ CAAAGAGGAATCCAGGGGCTAAAATGACC 3′

察される細胞，すなわち遺伝子導入された細胞を選択し，電位依存性膜容量の計測を行った．野生型の遺伝子を導入した細胞は，Prestin の機能に由来する特徴的なベル型非線形な膜容量を示す．Prestin に由来する非線形な膜容量は，

$$C_m(V) = C_{lin} + \frac{Q_{max}}{\alpha e^{\frac{V-V_{1/2}}{\alpha}}\left(1+e^{-\frac{V-V_{1/2}}{\alpha}}\right)^2} \quad (1)$$

に示すボルツマン関数によくフィッティングすることが知られている．ここで，C_{lin} は膜容量の線形成分，Q_{max} は電荷移動量の最大値，α は傾斜因子，$V_{1/2}$ は Prestin の半分が活性化される電位である．得られた Q_{max} を C_{lin} で割り，単位細胞膜面積当たりの Prestin の最大電荷輸送量を意味する charge density を求めた．

また，細胞膜単位体積当たりの非線形膜容量を評価するために，面積で規格化した非線形膜容量を以下のように定義する．

$$C_{nonlin/lin}(V) = \frac{C_{nonlin}}{C_{lin}} = \frac{\left(C_m(V) - C_{lin}\right)}{C_{lin}} \quad (2)$$

ここで，C_{nonlin} は膜容量の非線形成分である．また，変異体のデータと野生型のデータを比較するために，計測されたデータを野生型の $C_{nonlin/lin}$ の最大値でデータを規格化し，Relative $C_{nonlin/lin}$ と定義した．

C. 研究結果

C. 1. 脱糖鎖酵素の影響

図 6 に N 末端細胞内領域欠損 Prestin，STAS ドメイン欠損 Prestin 及び GTSRH 配列に関する変異体の Western blotting の結果を示す．FLAG 融合型野生型 Prestin，FLAG 融合型 N 末端細胞内領域欠損 Prestin，FLAG 融合型 STAS ドメイン欠損 Prestin，GTSRH 配列に関する FLAG 融合型変異体の理論分子量はそれぞれ 84.6 kDa，75.4 kDa，63.6 kDa，84.6 kDa である．酵素処理していない野生型 Prestin では約 100 kDa のシャープなバンドと約 70 kDa のスメアなバ

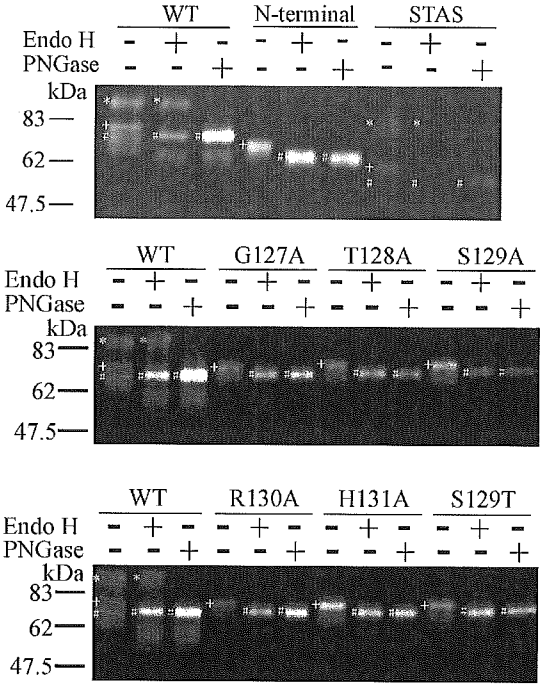

図 6. Western blotting の結果. Endo H は高マンノース型の糖鎖のみを，PNGase は複合型糖鎖を含むすべての糖鎖をタンパク質から取り除く酵素である．+，-はそれぞれ酵素処理したサンプル，していないサンプルを示す．＊は複合型糖鎖が結合した Prestin の，＋は高マンノース型糖鎖が結合した Prestin の，そして＃は糖修飾を受けていない Prestin のバンドを示している．

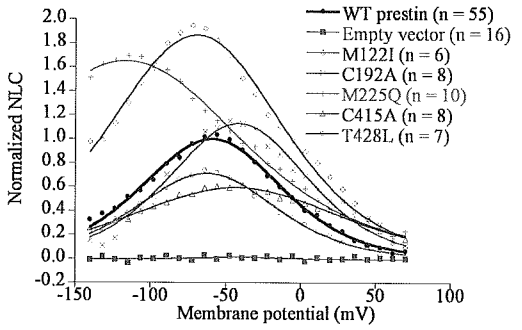

図 7. Prestin 特有のアミノ酸に関する変異体から得られたパッチクランプの結果. これら変異体では，非線形膜容量が計測され，これらは機能を維持していることが明らかになった．

ンドが検出された．Endo H により酵素処理すると約 100 kDa のバンドは変化しなかったが，スメアな約 70 kDa のバンドは輝度の高いシャープな 70 kDa のバンドに変化した．PNGase により酵素処理した際は，約 100 kDa のバンドが消え，輝度の高いシャープな 70 kDa のバンドのみが検出された．一方で，N 末端細胞内領域欠損 Prestin では，酵素処理していない場合，約 65 kDa のバンドのみが検出された．Endo H で酵素処理した場合，PNGase で処理した場合，共に，約 65 kDa のバンドは約 60 kDa にシフトした．また，STAS ドメイン欠損 Prestin では，約 80 kDa のシャープなバンドと約 50 kDa のスメアなバンドが検出された．Endo H により酵素処理すると約 80 kDa のバンドは変化しなかったが，スメアな約 50 kDa のバンドはシャープな 50 kDa のバンドに変化した．PNGase により酵素処理した際は，約 80 kDa のバンドが消え，輝度の高いシャープな 50 kDa のバンドのみが観測された．一方で，GTSRH に関する変異体では，酵素処理していない場合，約 80 kDa のバンドのみが検出された．Endo H で酵素処理した場合，PNGase で処理した場合，共に，約 80 kDa のバンドは約 70 kDa にシフトした．

C. 2. 変異 Prestin の機能評価

野生型 Prestin の遺伝子を含んだベクター，Prestin 遺伝子を挿入していない空のベクター，Prestin 特有のアミノ酸に関する変異体の遺伝子を含んだベクターをそれぞれ導入した HEK293 細胞から得られた細胞膜容量を図 7 に示す．空のベクターを導入した細胞では，膜電位の変化に対し，膜容量は一定の値になった．一方で，野生型 Prestin 遺伝子を挿入したベクター，Prestin 特有のアミノ酸に関する変異体の遺伝子挿入したベクターをそれぞれ導入した細胞では，非線形膜容量が計測された．計測されたフィッティングパラメータを

Fig. 8 に示す．αでは，M122I と M225Q は野生型 Prestin よりも有意に大きかった．$V_{1/2}$では，M122I と M225Q は野生型 Prestin よりも有意に小さく，C415A は有意に大きかった．Charge density では，M122I と M225Q が野生型 Prestin よりも有意に大きかった．

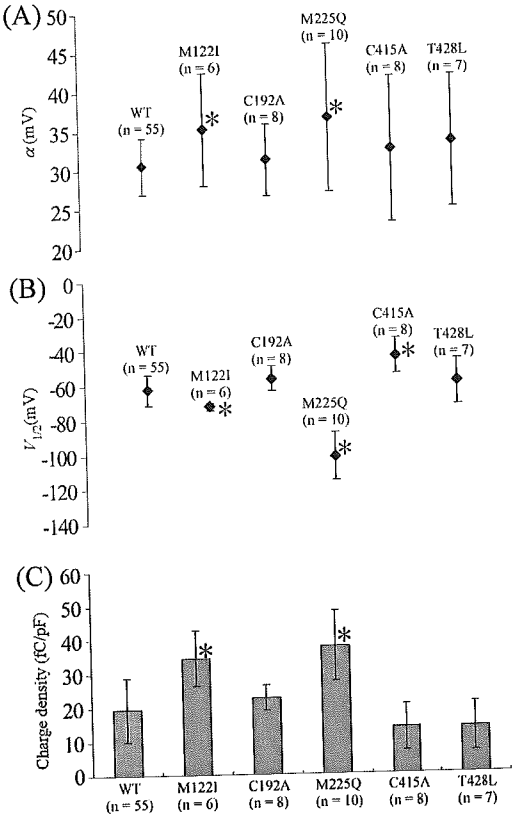

図 8. 非線形膜容量が計測された野生型及び変異体のフィッティングパラメータ．(A) α. Prestin の電位に対する敏感さを表すαは M122I, M225Q で野生型に対し有意に変化した．(B) $V_{1/2}$. Prestin がもっとも敏感に反応する膜電位を表す $V_{1/2}$ は M122I, M225Q で有意に変化した．(C) Charge density. 単位細胞膜面積当たりの Prestin の最大電荷輸送量を意味する charge density は M122I, M225Q では有意に上昇した．＊は野生型と変異体の間に有意差があることを示す．

D. 考察

D.1. 糖修飾の検討

脱糖鎖処理後の Western blotting の結果において，野生型 Prestin では，約 100 kDa のバンドは複合型糖鎖が結合した Prestin を，幅の広い約 70 kDa のバンドは高マンノース型の糖鎖が結合した Prestin 及び糖鎖の結合していない Prestin を示していると考えられた．すなわち，野生型 Prestin の遺伝子を導入した細胞には，複合型糖鎖が結合した Prestin，高マンノース型の糖鎖が結合した Prestin 及び糖鎖の結合していない Prestin が存在していると考えられた．約 70 kDa のバンドがスメアになっているのは，高マンノース型の糖鎖が結合した Prestin のバンドと糖鎖の結合していない Prestin のそれが重なっているためだと推察された．STAS ドメイン欠損 Prestin では，約 80 kDa のバンドは複合型糖鎖が結合した Prestin を，約 50 kDa のバンドは高マンノース型の糖鎖が結合した Prestin 及び糖鎖の結合していない Prestin を示していると考えられた．すなわち，STAS ドメイン欠損 Prestin の遺伝子を導入した細胞では，野生型同様 3 種類存在していることが示唆された．一方，N 末端細胞内領域欠損 Prestin では，約 65 kDa のバンドは高マンノース型の糖鎖が結合した Prestin を示していると考えられた．GTSRH に関する点変異体では，約 80 kDa のバンドは高マンノース型の糖鎖が結合した Prestin を示していると推察された．すなわち，N 末端細胞内領域欠損 Prestin または GTSRH に関する点変異体の遺伝子を導入した細胞では，高マンノース型の糖鎖が結合した変異 Prestin のみが存在していることが示唆された．

複合型糖鎖の結合の有無は，糖修飾を受けるアスパラギン（N）が糖を付加する酵素と反応しやすい位置に存在するかが大きく関わ

ってくる．変異による糖鎖の変化は，変異によりタンパク質の構造が変化し，糖修飾を受けるアミノ酸のタンパク質内での位置が変化したためであると考えられた．このことから，N 末端細胞内領域及び GTSRH 配列が Prestin の構造に大きく関わっていることが示唆された．

糖鎖がついていない Prestin のバンドは理論分子量よりも低い位置に現れている．これは Prestin が 12 回細胞膜を通過するタンパク質であり疎水性のアミノ酸が多く存在することに起因すると考えられる．つまり電気泳動によりタンパク質を分離する際，負の電荷をもった SDS が一般的なタンパク質に比べ多く Prestin に結合したことで陽極側に強く引かれ，Prestin がより早く下に流れると考えられた．この結果，理論分子量よりも低い位置にバンドが現れたと考えられた．

D.2. 変異 Prestin の機能

変異体が野生型 Prestin 同様，非線形膜容量を示した結果は，変異体がアニオン輸送機能を維持していることを示している．Prestin の電位に対する敏感さを表すαは M122I 及び M225Q が野生型に対し有意に変化した．Prestin がもっとも敏感に反応する膜電位を表す $V_{1/2}$ は M122I, M225Q 及び C415A が野生型に対し有意に変化した．αや $V_{1/2}$ が変異によって変化したという結果は，変異をかけたアミノ酸が Prestin の電位感受性に密接に関わっていることを示唆している．さらに単位細胞膜面積当たりの Prestin の最大電荷輸送量を意味する charge density は M122I 及び M225Q では有意に上昇した．Charge density の有意な上昇は，変異により Prestin の発現量が上昇した，あるいは一つの Prestin が運ぶ電荷の量が上昇したと考えられた．システイン（C）はシステイン同士でタンパク質の構造を決める上で重要なジスルフィド結合を作る可能性があることが知られている．しかし，本研究で作製した C192A 及び C415A はともにアニオン輸送機能を維持した．この結果は，C192 と C415 がジスルフィド結合を作らないことを示していると考えられた．

E. 結論

本研究で以下のことが示唆された．

1. N 末端細胞内領域及び GTSRH 配列に変異を加えると，Prestin の構造が変化する．

2. M122 をイソロイシン（I）に，または M225 をグルタミン（Q）に変異させるとアニオン輸送機能が増加する．

3. C192 と C415 がジスルフィド結合を作らない．

F. 健康危険情報

なし

G. 研究発表

論文発表

1. Murakoshi, M., Yoshida, N., Iida, K., Kumano, S., Kobayashi, T. and Wada, H., 2006. Local Mechanical Properties of Mouse Outer Hair Cells: Atomic Force Microscopic Study, *Auris Nasus Larynx*, in press.

2. Andoh, M., Nakajima, C. and Wada, H., Phase of Neural Excitation Relative to Basilar Membrane Motion in the Organ of Corti: Theoretical Considerations. *J. Acoust. Soc. Am.*, 2005, 118, 1554-1565.

3. Iida, K., Tsumoto, K., Ikeda, K., Kumagai, I., Kobayashi, T. and Wada, H., Construction of an Expression System for the Motor Protein Prestin in Chinese Hamster Ovary Cells. *Hear. Res.*, 2005, 205, 262-270.

4. Kumano, S., Iida, K., Murakoshi, M., Naito, N., Tsumoto, K., Ikeda, K., Kumagai, I., Kobayashi, T. and Wada, H., Effects of Mutation in the Conserved GTSRH Sequence of the Motor Protein Prestin on Its Characteristics. *JSME Int. J.*, 2005, 48C, 403-410.

学会発表

1. Iida, K., Murakoshi, M., Kumano, S., Tsumoto, K., Ikeda, K., Kumagai, I., Kobayashi, T., and Wada, H., Heterogeneous Expression of the Motor Protein Prestin. The 6th International Symposium on Future Medical Engineering based on Bio-nanotechnology, Sendai, Japan (November 2005).

2. Kumano, S., Iida, K., Murakoshi, M., Naito, N., Tsumoto, K., Ikeda, K., Kumagai, I., Kobayashi, T. and Wada, H., The Role of the Conserved GTSRH Sequence of the Motor Protein Prestin in Its Characteristics. The 2nd Asian Pacific Conference on Biomechanics, Taipei, Taiwan (November 2005).

3. Murakoshi, M., Kitsunai, Y., Yoshida, N., Kobayashi, T. and Wada, H., Protection of outer hair cells from traumatic noise by prior whole-body heat stress, The 2nd Asian Pacific Conference on Biomechanics, Taipei, Taiwan (November 2005).

4. Murakoshi, M., Kitsunai, Y., Yoshida, N., Kobayashi, T. and Wada, H., Changes in Structure and Mechanical Properties of Mouse Outer Hair Cells in Response to Whole-body Heat Stress, The Second Japan-Switzerland Workshop on Biomechanics, Kyoto, Japan (September 2005)

5. Murakoshi, M., Iida, K., Kumano, S., Yoshida, N., Kobayashi, T. and Wada, H., Heat stress-induced changes in the mechanical properties of mouse outer hair cells. The 9th "Mechanics of Hearing" Workshop, Portland, Oregon, U.S.A. (July 2005).

6. Wada, H., Murakoshi, M., Iida, K., Gomi, T., Kimura, K., Uskura, H., Sugawara, M., Katori, Y., Kakehata, S., Ikeda, K. and Kobayashi, T., Atomic force microscopic imaging of the intra cellular membrane surface of prestin-expressing Chinese hamster ovary cells. The 9th "Mechanics of Hearing" Workshop, Portland, Oregon, U.S.A. (July 2005).

7. 飯田浩司, 熊野峻, 村越道生, 津本浩平, 池田勝久, 熊谷泉, 小林俊光, 和田仁. 蝸牛外有毛細胞に存在するタンパク質モータ prestin の精製とその機能評価. 日本機械学会第 18 回バイオエンジニアリング

講演会, 新潟 (2006 年 1 月).

8. 熊野峻, 飯田浩司, 村越道生, 津本浩平, 池田勝久, 熊谷泉, 小林俊光, 和田仁. "部位特異的変異導入によるタンパク質モータ prestin の保存配列 GTSRH の解析. 日本機械学会第 18 回バイオエンジニアリング講演会, 新潟 (2006 年 1 月).

9. 村越道生, David Z.Z. He, 飯田浩司, 熊野峻, 和田仁. 電位依存性タンパク質モータ prestin の構造変化観察. 日本機械学会第 18 回バイオエンジニアリング講演会, 新潟 (2006 年 1 月).

10. 飯田浩司, 津本浩平, 池田勝久, 熊谷泉, 小林俊光, 和田仁. タンパク質モータ prestin の安定発現細胞株の構築と高発現株の選択, 第 28 回日本バイオレオロジー学会年会, 仙台 (2005 年 7 月).

11. 村越道生, 吉田尚弘, 小林俊光, 和田仁. ヒートストレスによるマウス外有毛細胞の機械的特性の変化, 第 28 回日本バイオレオロジー学会年会, 仙台 (2005 年 7 月)

H. 知的財産権の出願・登録状況

なし.

研究成果の刊行に関する一覧表

発表者氏名	論文タイトル	発表誌名	巻号	ページ	出版年
Murakoshi, M., Yoshida, N., Iida, K., Kumano, S., Kobayashi, T. and Wada, H.	Local Mechanical Properties of Mouse Outer Hair Cells: Atomic Force Microscopic Study	Auris Nasus Larynx	In press		
Andoh, M., Nakajima, C. and Wada, H.	Phase of Neural Excitation Relative to Basilar Membrane Motion in the Organ of Corti: Theoretical Considerations.	J. Acoust. Soc. Am.	118	1554-1565	2005
Iida, K., Tsumoto, K., Ikeda, K., Kumagai, I., Kobayashi, T. and Wada, H.	Construction of an Expression System for the Motor Protein Prestin in Chinese Hamster Ovary Cells.	Hear. Res.	205	262-270	2005
Kumano, S., Iida, K., Murakoshi, M., Naito, N., Tsumoto, K., Ikeda, K., Kumagai, I., Kobayashi, T. and Wada, H.	Effects of Mutation in the Conserved GTSRH Sequence of the Motor Protein Prestin on Its Characteristics.	JSME Int. J.	48C	403-410	2005

ELSEVIER

Auris Nasus Larynx xxx (2006) xxx–xxx

AURIS NASUS LARYNX
INTERNATIONAL JOURNAL OF ORL & HNS

www.elsevier.com/locate/anl

Local mechanical properties of mouse outer hair cells: Atomic force microscopic study

Michio Murakoshi [a,*], Naohiro Yoshida [b], Koji Iida [a], Shun Kumano [a], Toshimitsu Kobayashi [b], Hiroshi Wada [a]

[a] *Department of Bioengineering and Robotics, Tohoku University, 6-6-01 Aoba-yama, Sendai 980-8579, Japan*
[b] *Department of Otorhinolaryngology, Head and Neck Surgery, Tohoku University Graduate School of Medicine, 1-1 Seiryo-machi, Sendai 980-8574, Japan*

Received 16 June 2005; accepted 11 November 2005

Abstract

Objectives: Outer hair cells (OHCs) are capable of altering their cell length in response to changes in membrane potential. Due to this electromotility, OHCs probably subject the basilar membrane to force, resulting in cochlear amplification. To understand the mechanism of such amplification, knowledge of the mechanical properties of OHCs is required since the force produced by OHC electromotility is thought to depend on such properties. Various studies have been conducted to investigate the mechanical properties of guinea pig OHCs. With regard to mice, however, although various kinds of transgenic and knockout mice possess great potential as research models, the mechanical properties of mouse OHCs have not as yet been reported since the cells and/or tissues in the mouse hearing organ are relatively small and vulnerable to external stimuli, rendering sample preparation difficult. In this study, therefore, to establish indicators of the mechanical properties of OHCs in mice, such properties were measured by atomic force microscopy (AFM).
Methods: CBA/JNCrj strain male mice aged 10–12 weeks (25–30 g) were used. Cochleae were dissected out from the animal and both the basilar membrane and the organ of Corti were simultaneously unwrapped from the modiolus with forceps. Dissected coiled tissue was then incubated with an enzymatic digestion medium for 15 min. After digestion, OHCs were isolated by gently triturating the coiled tissue. Local mechanical properties of the OHCs were then measured by an indentation test using an AFM.
Results: Young's modulus and stiffness of the OHC in the apical turn of the mouse cochlea were 2.1 ± 0.5 kPa and 4.4 ± 1.2 mN/m, respectively.
Conclusions: Young's modulus of the OHC in the apical turn of the cochlea in mice was roughly the same as that in the apical turn of the cochlea in guinea pigs; however, the stiffness of the former was about two times greater than that of the latter because the cell length of the former was shorter than that of the latter.

Keywords: Mouse; Outer hair cell; Local mechanical property; Atomic force microscopy

1. Introduction

Hearing in mammals is characterized by high sensitivity, wide dynamic range and sharp frequency selectivity. These remarkable profiles are realized by the well-ordered system of the hearing organ. When sound enters the ear, it is transmitted through the outer and middle ears and finally causes vibration of the stapes. This mechanical vibration of the stapes generates pressure fluctuation of the cochlear fluid across the basilar membrane, the stiffness of which decreases from the base toward the apex of the cochlea, creating traveling waves on the membrane [1]. Outer hair cells (OHCs), which are located on the basilar membrane as a part of the organ of Corti, were found to be motile by previous in vitro studies [2–6]. Based on these experiments, OHCs are thought to respond to acoustical stimulation from the outer and middle ear with elongation and contraction of their cylindrical soma in vivo. Due to this motility, OHCs are thought to subject the basilar membrane to force, causing

* Corresponding author. Tel.: +81 22 795 4048; fax: +81 22 795 6939.
E-mail address: michio@wadalab.mech.tohoku.ac.jp (M. Murakoshi).

0385-8146/$ – see front matter © 2005 Elsevier Ireland Ltd. All rights reserved.
doi:10.1016/j.anl.2005.11.009

amplification of the amplitude of basilar membrane vibration, i.e., cochlear amplification, leading to refinement of the sensitivity, dynamic range and frequency selectivity of mammalian hearing.

To understand the active mechanism of this hearing system, knowledge of the mechanical properties of OHCs is required since such properties are essential to the overall behavior of the organ of Corti in the cochlea. Intensive research seeking to elucidate such properties has been conducted using various kinds of experimental techniques. Zenner et al. reported the axial stiffness of the OHC using cell capillaries [7]. Employing calibrated glass fibers, Hallworth reported the axial compliance [8] and Ulfendahl et al. revealed that the axial stiffness is lower than the transverse stiffness of the OHC [9]. Tolomeo et al. applied glass pipettes for three-point bending measurements and obtained the axial stiffness of the OHC [10]. Oghalai et al. characterized the stiffness of the lateral wall of the OHC by a micropipette aspiration technique [11], and Bata et al. subsequently reported such stiffness using a similar technique [12]. Using flexible vibration fibers, He and Dallos measured the dynamic stiffness of the OHC, namely, the decrease in the axial stiffness of the cell due to depolarization and its increase due to hyperpolarization [13]. These reports addressed the whole-cell stiffness rather than the local mechanical properties of the OHC lateral wall. Sugawara et al. elucidated Young's modulus of the isolated OHC [14] and that of the inner hair cells and other cells in the organ of Corti [15] by atomic force microscopy (AFM). Recently, Zelenskaya et al. reported the viscoelastic properties of the OHC lateral wall as well as its stiffness properties as observed by AFM [16].

Mice are one of the most widely employed research animals since they have several advantages as experimental animal models. One such advantage is that many types of inbred strains, each of which possesses a gene that causes physiologically interesting characteristics, have been developed. It has also become possible to produce a variety of new types of transgenic and knockout mice using genetic-engineering techniques. With the availability of specific mice, mice have become a powerful tool for genetic research. Secondly, since there is a high homology between mouse and human genomes, in some cases, an orthologous gene is involved in the same disease, including hearing impairment, in the two species. The genomic approach using mice is thus feasible for studying human diseases. Thirdly, in 2002, the full-length mouse complementary DNA sequences were revealed by the FANTOM Consortium and the RIKEN Genome Exploration Research Group Phase I & II Team [17], making mice the experimental vertebrate with the best characterized genome to date. Thus, auditory research on mice can possibly lead to findings pertinent to not only basic but also clinical research on hearing. However, mice are seldom used in hearing research. Experiments using hearing organ tissues and/or cells, for example, are mostly limited to guinea pigs because the inner ear of guinea pigs is relatively large compared with its body weight, and thus preparation of the cells is easy. Moreover, in mice, the OHCs in the hearing organ are small and susceptible to external stimuli, and their connections with the cells are tight. Thus, isolation of OHCs is difficult. Hence, the mechanical properties of mouse OHCs have not yet been clarified.

In the present study, therefore, to establish indicators of the mechanical properties of OHCs in mice, isolation of OHCs from mice was attempted and the local mechanical properties of mouse OHCs were measured by AFM.

2. Materials and methods

2.1. Cell preparation

CBA/JNCrj strain male mice aged 10–12 weeks (25–30 g) were used. Animals were decapitated and their bullae were detached and kept in a tissue culture medium (Leibovitz's L-15, Invitrogen, Carlsbad, CA) at 4 °C, which had been adjusted to pH 7.3 and 331 mOsm. Cochleae were dissected out from the bullae and transferred into another tissue culture medium. The bony shell covering the cochlea was then removed from the oval window toward the apex by an angled pick with sharpened tip, and both the basilar membrane and the organ of Corti were simultaneously unwrapped from the basal end of the modiolus toward its apical end with forceps. Dissected coiled tissue was then severed into two pieces, i.e., the apical turn and the basal turn, and only the apical turn was used as a specimen in this study since the cells located at the basal turn of the organ of Corti are vulnerable to external stimuli and thus had possibly been destroyed when the coiled tissue was dissected from the cochlea. The tissue was then transferred to an enzymatic digestion medium which contained 1 ml of the culture medium and 1 mg of type IV collagenase (Sigma–Aldrich, St. Louis, MO). This digestion medium had been prepared before dissection and maintained at 37 °C inside an incubator. After incubation for 15 min with the enzymatic digestion medium, the tissue was transferred into an enzyme-free culture medium in glass-bottomed dishes, the glass surface of which was coated with poly-D-lysine (MatTek, Ashland, MA). Solitary OHCs were isolated by gentle trituration of the coiled tissue in that medium with a 200-μl pipette and then left at rest for a few minutes to allow attachment of the isolated cells to the bottom of the dish. For the subsequent AFM measurement, the cells showing no obvious signs of deterioration such as shrinkage, swelling and/or translocation of the nucleus were selected and measurement was carried out within 1 h after the isolation of OHCs from the organ of Corti. All experiments were performed at room temperature.

The care and use of the animals in this study were approved by the Institutional Animal Care and Use Committee of Tohoku University, Sendai, Japan.

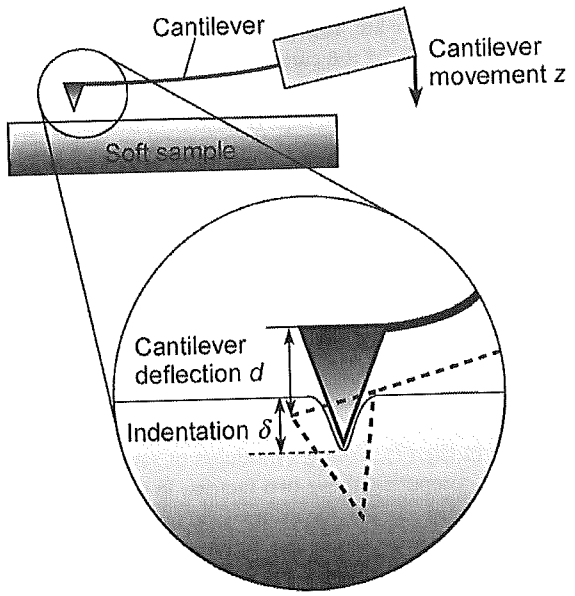

Fig. 1. A schema of the cantilever on a soft sample. When the tip of the cantilever touches the soft sample, the cantilever starts to deflect and then the deflection of the cantilever is optically detected by a laser system. By this measurement, the relationship between the movement of the cantilever z driven by a piezoelectric scanner and the cantilever deflection d was obtained.

2.2. *Atomic force microscopy*

An AFM (NVB100, Olympus, Tokyo, Japan) was used for the experiments. As the AFM unit is mounted on an inverted optical microscope, positioning of the tip above the cells is easy. V-shaped silicon nitride cantilevers (OMCL-TR400PSA-2, Olympus, Tokyo, Japan) with a pyramidal tip and a spring constant of 0.08 N/m were used. The typical radius of the curvature of the tip was less than 20 nm. Fig. 1 depicts the principal of an indentation test using the AFM. When the cantilever is moved by a piezoelectric scanner and the tip of the cantilever comes in contact with the sample, the cantilever starts to deflect, such deflection being optically detected by a laser system, which is composed of a laser, a mirror and a photodiode array. Due to this measurement, the relationship between the movement of the cantilever z driven by the piezoelectric scanner and the cantilever deflection d was obtained. This obtained curve is termed "force curve" because the force applied to the sample can be calculated by multiplying the cantilever deflection d by the spring constant of the cantilever. In each measurement, the hysteresis between two force curves, i.e., the curve obtained when the tip pushes against the sample and the curve obtained when the tip retracts from the sample, was ascertained. Because the deviations of the curves were confirmed to be negligible, the sample was kept elastic during the measurement. Fig. 2 shows an OHC isolated

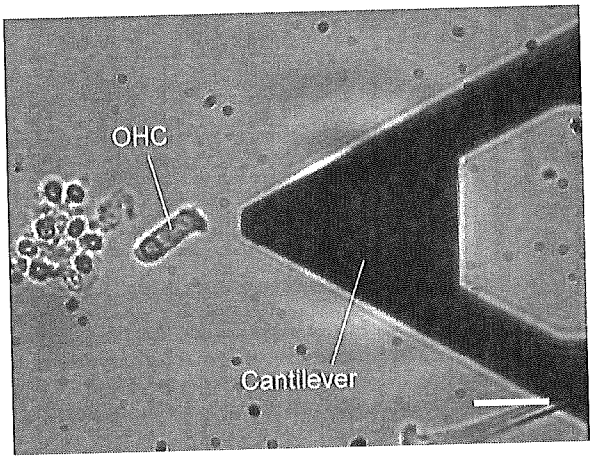

Fig. 2. Photomicrograph of an isolated OHC and the cantilever. The OHC was dissected from the apical turn of the cochlea in mice. Scale bar is 20 μm.

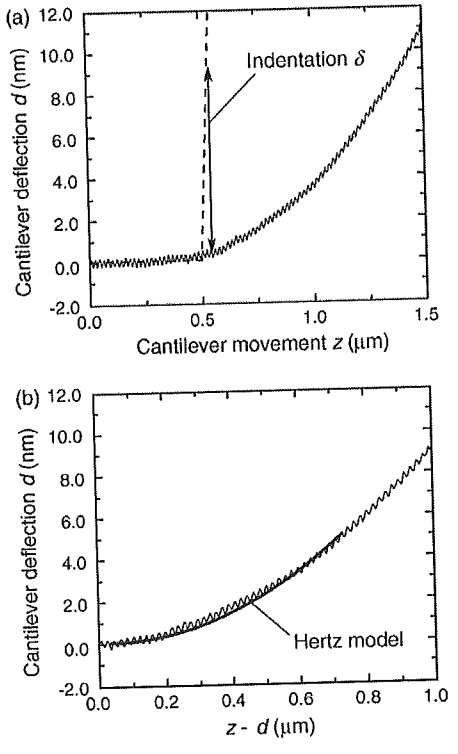

Fig. 3. Measurement data of cantilever deflection. (a) Relationship between the cantilever deflection d and cantilever movement z, i.e., force curve, obtained from both a hard sample (substrate) and a soft sample (OHC). (- - - -), hard sample; (—), soft sample. In the case of the hard sample, the cantilever deflection remains steady at zero until the cantilever touches the sample, at which time it rises proportionately with the increase in the cantilever movement. The vertical arrow shows the indentation δ, i.e., the difference between the cantilever deflection of the hard sample and that of the soft sample. (b) Relationship between the cantilever deflection d and the difference between the cantilever movement z and cantilever deflection d, i.e., $(z - d)$. The thin line shows the experimental data. The thick line represents the square regression line fitted by Eq. (5).

from the apical turn of the mouse cochlea and the cantilever.

2.3. Analysis of force curves

Examples of force curves obtained from both hard (substrate) and soft (OHC) samples are shown in Fig. 3(a). In the case of the hard sample, the cantilever deflection d remains steady at zero until the cantilever touches the sample, at which time it rises proportionately with the increase in the cantilever movement z. Regarding the case of the soft sample, the cantilever deflection d increases gradually after the cantilever touches the sample since the tip of the cantilever indents the sample; however, distinguishing the contact point between the sample and the tip of the cantilever is difficult. Thus, the contact point was numerically determined as described previously [15]. Assuming that the contact point is (z_0, d_0), the cantilever movement and the cantilever deflection after the cantilever contacts the sample, namely, post-contact cantilever movement z' and post-contact cantilever deflection d', are written as follows:

$$z' = z - z_0 \tag{1}$$

$$d' = d - d_0 \tag{2}$$

As the difference between the post-contact cantilever movement z' and the post-contact cantilever deflection d' indicates the sample indentation, the indentation δ is given by

$$\delta = z' - d' \tag{3}$$

Substituting Eqs. (1) and (2) into Eq. (3), the indentation δ is obtained as follows:

$$\delta = z' - d' = (z - z_0) - (d - d_0) \tag{4}$$

Fig. 3(b) shows the relationship between the cantilever deflection d and the difference between the cantilever movement z and the cantilever deflection d, i.e., $(z - d)$, which is obtained from Fig. 3(a). The curve in this figure is fitted with a square regression line, which is given by

$$d = a\{(z - d) - b\}^2 + c \tag{5}$$

The parameters a, b and c are obtained by the least squares method, in which a is the slope of the curve and represents the elastic properties of the sample; that is, the harder the sample, the greater the deflection of the cantilever, resulting in a larger value of slope a. When samples are elastic, isotropic, homogeneous and semi-infinite, and the indentation tip is rigid and conical, the Hertz model, which describes the elastic response of such subjects indented by the tip, can be applied to the measurement data. According to the Hertz model, the relationship between the post-contact cantilever deflection d' and the indentation δ is defined as follows:

$$d' = \{2E \tan\alpha/\pi k(1 - \nu^2)\}\delta^2 \tag{6}$$

where E, α, k and ν are Young's modulus of the sample, the half-opening angle of the cantilever, the spring constant of the cantilever and Poisson's ratio of the sample, respectively [18,19]. The substitution of Eqs. (2) and (4) into Eq. (6) leads to the following equation:

$$d = \{2E \tan\alpha/\pi k(1 - \nu^2)\}\{(z - d) - (z_0 - d_0)\}^2 + d_0 \tag{7}$$

In this study, the half-opening angle and the spring constant of the cantilever were 17° and 0.08 N/m, respectively. Poisson's ratio was assumed to be 0.499 because the samples were biomaterials, i.e., incompressible materials. Since slope a in Eq. (5) corresponds to the coefficient $2E \tan\alpha/\pi k(1 - \nu^2)$ in Eq. (7), Young's modulus of sample E can be obtained by comparing these two factors. In addition, as the parameters b and c in Eq. (5) correspond to $(z_0 - d_0)$ and d_0 in Eq. (7), respectively, the contact point (z_0, d_0) is simultaneously determined.

3. Results

3.1. Location-dependent variance of mechanical properties

Mechanical properties of the OHC in the apical turn of the cochlea were measured at various points along the longitudinal axis of the OHC. In this measurement, since the

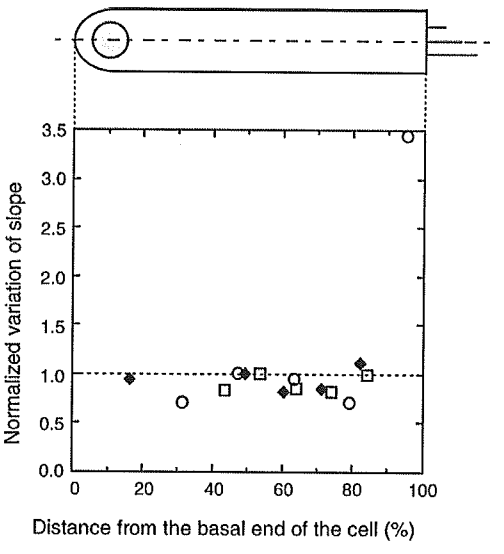

Fig. 4. Variance of the mechanical properties of OHCs along the longitudinal axis. The vertical axis represents the slope of the square regression line at the point of measurement divided by that in the middle part of the cells, and the horizontal axis shows the percentage of the distance of each measurement point from the basal end of the OHC, i.e., positions of the basal and apical ends along the cell axis are represented as 0% and 100%, respectively. The different symbols indicate the data obtained from different cells ($n = 3$). The inset represents the measurement position on the cell.

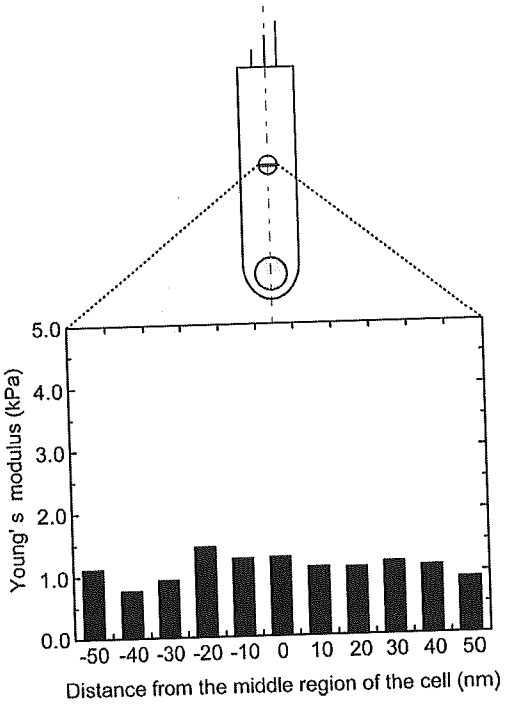

Fig. 5. Distribution of the mechanical properties of an OHC along the circumferential direction. The vertical axis represents Young's modulus and the horizontal axis shows the distance from the middle region of the measured OHC. Measurements were performed at 11 points at intervals of 10 nm. The mean and standard deviation of Young's modulus were 1.1 ± 0.19 kPa. The inset represents the measurement position on the cell.

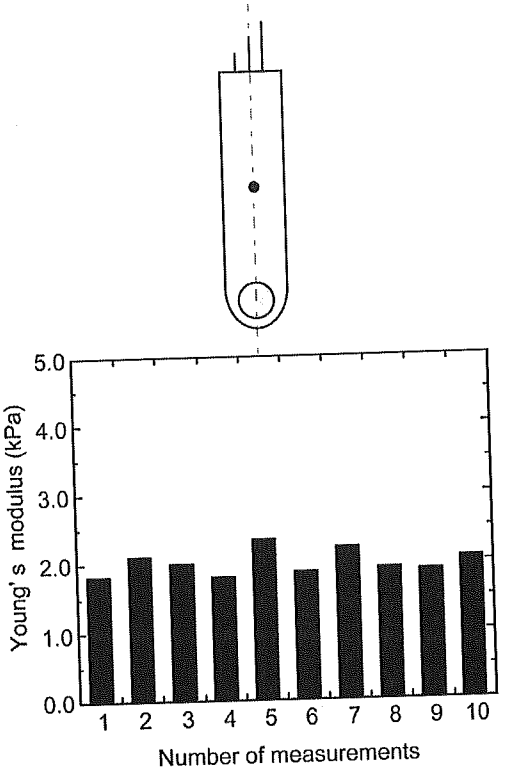

Fig. 6. Young's modulus obtained 10 times at one point in the middle region of the OHC. Young's modulus of OHCs obtained from the apical turn of the cochlea was measured 10 times at one point in the middle region of the OHC. The mean and standard deviation of Young's modulus were 2.0 ± 0.18 kPa. The inset represents the measurement position on the cell.

surface profile of the apical region of the OHC could not be regarded as semi-infinite in extent, the obtained data could not be analyzed by the Hertz model. The relationships between the cantilever deflection and the indentation of the OHC were therefore measured and the slopes of the square regression lines fitted to these relationships were obtained. Fig. 4 shows the relationship between the slope and the distance from the basal end of the OHC ($n = 3$). The horizontal axis represents the percentage of the distance of each measurement point from the basal end of the OHC, i.e., positions of the basal and apical ends along the cell axis are represented as 0% and 100%, respectively. The vertical axis shows the normalized variation of the slope, i.e., the value of the slope at each point divided by that in the middle part of the cell. From this figure, it can be seen that there was no significant difference in the mechanical properties in the region between 10% and 90% from the basal end of the cell. Hence, all measurements in the following experiments were conducted in the middle region of the OHC.

As shown in Fig. 5, variance of mechanical properties according to the location in the circumferential direction was evaluated. Measurements were performed in the middle region of an apical turn OHC at 11 points at intervals of 10 nm in the circumferential direction. The mean and standard deviation of Young's modulus were 1.1 ± 0.19 kPa. Variance of mechanical properties due to the repeated measurement at one point was then assessed as shown in Fig. 6. When Young's modulus was measured 10 times at one point in the middle region of the OHC, the mean and standard deviation of Young's modulus were 2.0 ± 0.18 kPa. No significant difference was seen between the variance of Young's modulus obtained from different points along the circumferential direction and that obtained from the repeated measurement. These results imply that the variance of Young's modulus obtained for each cell is due to repetition of the measurement rather than the location of the measurement point. Thus, to reduce this variance of Young's modulus and to take the limited measurable time of this experiment into account, force curves were obtained at one point, i.e., the central part of the middle region of the OHC, and the mean value of four Young's moduli measured at that point were defined as Young's modulus of the OHC.

3.2. Local mechanical properties of mouse outer hair cells

The relationship between Young's modulus of the mouse OHCs in the apical turn and the cell length ($n = 10$) is shown in Fig. 7. Lengths of the apical turn OHCs ranged from 15.7 to 21.3 μm and their Young's moduli ranged from 1.3 to

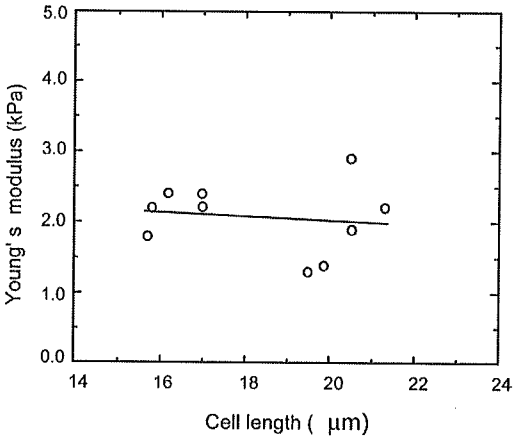

Fig. 7. Relationship between Young's modulus and the length of OHCs. Young's modulus and the cell length of OHCs ranged from 1.3 to 2.9 kPa and from 15.7 to 21.3 μm, respectively ($n = 10$). The regression line is given by $y = -0.025x + 2.5$ ($r = -0.11$). No significant correlation was observed between Young's modulus and the cell length.

2.9 kPa. The mean and standard deviation of Young's moduli of the apical turn OHCs were 2.1 ± 0.5 kPa. The regression line is given by $y = -0.025x + 2.5$ and the correlation coefficient r is -0.11. Thus, regarding OHCs in the apical turn of the mouse cochlea, no significant correlation was observed between Young's modulus and the cell length.

4. Discussion

4.1. Preparation process of outer hair cells

To measure the mechanical properties of the isolated mouse OHCs, it is essential to obtain isolated cells which are as intact as possible. The morphology of the cells was therefore microscopically examined as an index of cell intactness, and cells were selected for experiments only if they showed no obvious deterioration such as shrinkage, swelling and/or translocation of the nucleus.

In this study, the length of the selected OHCs ranged from 15.7 to 21.3 μm as shown in Fig. 7. Keiler and Richter reported the sizes of various elements in the cochlea of different strains of mice, including CBA/CaJ strain mice, by using the hemicochlea technique, which enables direct observation of cross sections of fresh mouse cochlea [20]. According to their report, the first, second and third rows of OHCs obtained from the apical turn of the cochlea of CBA/CaJ strain mice were 22.2 ± 1.4, 20.6 ± 1.3 and 19.9 ± 1.2 μm in length, respectively, i.e., the length of OHCs in the apical turn of the cochlea range from approximately 18 to 24 μm. The length of OHCs obtained in this study was 11–15% shorter than that reported in their study. Indeed, an isolated OHC with an initial length of 24.2 μm showed a gradual shortening of the cell soma, namely, the cell decreased in length to 20.7, 20.3 and 19.3 μm at 15, 25 and 45 min after isolation, respectively.

The difference in the length of OHCs between this study and Keiler and Richter's study is possibly due to differences in sample preparation; that is, OHCs were isolated from neighboring OHCs and supporting cells with enzymatic digestion and subsequent mechanical trituration using a pipette in this study, whereas a fresh cross section of the mouse hemicochlea was used as a specimen in the previous study. In this study, enzymatic isolation was carried out using type IV collagenase. Type IV collagen is a major structural component of the extracellular matrix, i.e., the basilar membrane in the organ of Corti [21]. Therefore, the influences of the enzymatic isolation with type IV collagenase on epithelial cells, i.e., OHCs in the organ of Corti, are negligibly small, suggesting that its effect on the mechanical properties of OHCs is also negligible. Although the isolation procedures applied in this study may have resulted in inevitable shrinkage of OHCs, the length change of the cell remained within 3.1 μm (13.8%), even though 45 min elapsed after isolation. Furthermore, cell morphology was microscopically fine without swelling and/or translocation of the nucleus. In this study, therefore, AFM measurement was deemed to be applicable to the isolated OHCs.

4.2. Atomic force microscopic analysis of Young's modulus of outer hair cells

Regarding the mechanical properties of OHCs, there have been various reports [7–13]. Recently, the mechanical properties of the sensory and supporting cells in the organ of Corti have been studied by AFM [14–16]. When Young's modulus of a sample is measured by AFM, the sample must be elastic, isotropic, homogenous and semi-infinite to accurately estimate Young's modulus by using a proper mathematical model, i.e., the Hertz model. In the present study, since no hysteresis was shown in the force curves between approach to and retraction from the sample, the sample was assumed to be elastic. Regarding the lateral wall of the OHC, it is considered to be orthotropic because of the existence of the actin-spectrin cortical lattice [22,23]. However, the OHC can be assumed to be isotropic when the indentation depth of the cell by the AFM tip is sufficiently large compared with the OHC diameter because Young's modulus measured by that means reflects the total of the orthotropic lateral wall and the isotropic cytoplasm of the cell rather than only the orthotropic lateral wall since the thickness of the lateral wall of the OHC is only several tens of nanometers [14]. In the present study, the diameter of the isolated mouse OHC was approximately 7 μm and the indentation depth of the cell by the cantilever tip was up to 1 μm. Thus, the sample was assumed to be isotropic. In addition, since Young's modulus was measured at the central part of the middle region of the OHC, where there are no prominent organelles such as the nucleus and endoplasmic

reticulum, the sample was assumed to be homogeneous. Moreover, when the radius of curvature of the indentation tip is sufficiently smaller than the thickness of the sample, the sample can be regarded as semi-infinite [24]. In this study, since the radius of the curvature of the cantilever tip was less than 20 nm, the semi-infinite sample assumption was satisfied. Thus, all assumptions with regard to application of the Hertz model are appropriate.

4.3. Difference in mechanical properties of OHCs between guinea pigs and mice

Although the stiffness of the guinea pig OHCs has been measured in many studies, the reported values vary from 0.147 to 25 mN/m depending on the measurements [7–10,13,14,16,25,26]. Therefore, in the present study, we compared the stiffness of the mouse OHCs with that of the guinea pig OHCs reported by the previous study [14] since the applied experimental method is identical to that of this study, i.e., an indentation test using an AFM.

Fig. 8 shows the relationship between Young's modulus and the length of the OHC obtained from mice in this study and such relationship obtained from guinea pigs investigated by Sugawara et al. [14]. As shown in this figure, Young's modulus of the mouse OHC in the apical turn of the cochlea had about the same value as that of the guinea pig OHC in the apical turn of the cochlea. The reason why the apical turn mouse OHCs had Young's moduli similar to the apical turn guinea pig OHCs is unknown. In general, Young's modulus depends only on material, not on shape. Thus, one possible reason for this similarity is the same morphology of the lateral wall of the OHC between mice and guinea pigs. However, there is a difference in subsurface-cisternal morphology between mice and guinea pigs; that is, the mouse OHC has only one layer of the subsurface cisternae (SSC), whereas the guinea pig OHC has a number of such layers [27,28]. Oghalai et al. reported that most of the lateral wall's resistance to local bending is realized by the existence of both the cortical lattice (CL) and the SSC [11]. Although to what degree the SSC contribute to OHC Young's modulus is unknown, fewer SSC layers in the mouse OHC probably resulted in Young's modulus of the mouse OHC being smaller than that of the guinea pig OHC. Based on these considerations, about the same values of Young's modulus between the mouse and guinea pig apical turn OHC imply that the morphology of the CL in the mouse OHC may also be different from that in the guinea pig OHC.

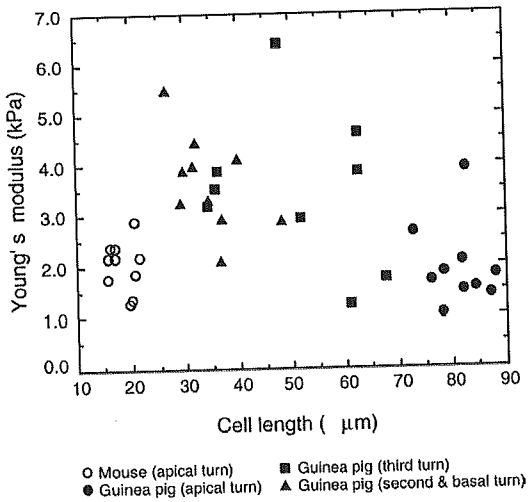

Fig. 8. Relationship between Young's modulus and the length of OHCs. Open circles represent OHCs obtained from the apical turn of the mouse cochlea in this study. Filled circles, filled squares and filled triangles represent OHCs obtained from the apical turn, the third turn and the second and basal turns of the guinea pig cochlea, respectively, as reported by Sugawara et al. [14]. Young's modulus of the OHC obtained from the apical turn of the mouse cochlea tended to be smaller and greater than those obtained from the basal turn and the apical turn of the guinea pig cochlea, respectively.

Focusing on the stiffness of the OHC, it can be evaluated from its Young's modulus by applying a simple one-dimensional model of the OHC as described previously [14]. Since isolated outer hair cells in vitro have a different condition in mechanical coupling compared with those in vivo, i.e., OHCs in vivo are connected with other OHCs, pillars, Deiters' cells, the extracellular matrix, the efferent system, etc., there is a possibility that the stiffness of OHCs in vitro differ from that of those in vivo. It has been reported that the motion of the basilar membrane included not only the AC component but also DC offset [29]. At a characteristic frequency region, the basilar membrane was displaced by about 0.2 nm toward the scala vestibuli. This compression may affect the mechanical properties of OHCs. However, the change of the OHC stiffness may be negligibly small because the 0.2-nm contraction of the OHC soma may induce a stiffness change in OHCs of only about 0.001% [13]. Assuming the cylindrical shape and homogeneity of the OHC, the stiffness of the OHC k_{cell} is shown by the following equation:

$$k_{cell} = \pi R^2 E / L \tag{8}$$

where R and L indicate the radius and length of the OHC, respectively. Derived from Eq. (8), the stiffness of the OHC in the apical turn of the mouse cochlea was estimated to be 4.4 ± 1.2 mN/m ($n = 10$), as shown in Table 1. Also shown is its Young's modulus measured in this study, as well as Young's modulus and the stiffness of the guinea pig OHC reported previously [14]. Comparing the data of the mouse OHC in the apical turn of the cochlea with those of the guinea pig OHC in the apical turn, although Young's modulus of the mouse OHC was roughly the same as that of the guinea pig OHC, the stiffness of the former is about two times greater than that of the latter.

In a general sense, the basilar membrane becomes wider and thinner with distance along the cochlea from base to apex, resulting in the graduation of its stiffness along the cochlear partition. Because of this stiffness gradient, traveling waves occur on the basilar membrane and thus